





Regulation of a pentameric ligand-gated ion channel by a semiconserved cationic lipid-binding site

Received for publication, March 23, 2021, and in revised form, June 10, 2021. Published, Papers in Press, June 19, 2021.
<https://doi.org/10.1016/j.jbc.2021.100899>

Akshay Sridhar^{1,‡}, Sarah C. R. Lummis^{2,‡}, Diletta Pasini³, Aujan Mehregan³, Marijke Brams³, Kumiko Kambara⁴, Daniel Bertrand⁴, Erik Lindahl^{1,5}, Rebecca J. Howard^{5,*}, and Chris Ulens^{3,*}

From the ¹Department of Applied Physics, Science for Life Laboratory, KTH Royal Institute of Technology, Solna, Sweden; ²Department of Biochemistry, University of Cambridge, Cambridge, United Kingdom; ³Laboratory of Structural Neurobiology, Department of Cellular and Molecular Medicine, Faculty of Medicine, KU Leuven, Leuven, Belgium; ⁴HiQScreen Sàrl, Geneva, Switzerland; ⁵Department of Biochemistry and Biophysics, Science for Life Laboratory, Stockholm University, Solna, Sweden

Edited by Mike Shipston

Pentameric ligand-gated ion channels (pLGICs) are crucial mediators of electrochemical signal transduction in various organisms from bacteria to humans. Lipids play an important role in regulating pLGIC function, yet the structural bases for specific pLGIC-lipid interactions remain poorly understood. The bacterial channel ELIC recapitulates several properties of eukaryotic pLGICs, including activation by the neurotransmitter GABA and binding and modulation by lipids, offering a simplified model system for structure–function relationship studies. In this study, functional effects of noncanonical amino acid substitution of a potential lipid-interacting residue (W206) at the top of the M1-helix, combined with detergent interactions observed in recent X-ray structures, are consistent with this region being the location of a lipid-binding site on the outward face of the ELIC transmembrane domain. Coarse-grained and atomistic molecular dynamics simulations revealed preferential binding of lipids containing a positive charge, particularly involving interactions with residue W206, consistent with cation- π binding. Polar contacts from other regions of the protein, particularly M3 residue Q264, further support lipid binding *via* headgroup ester linkages. Aromatic residues were identified at analogous sites in a handful of eukaryotic family members, including the human GABA_A receptor ϵ subunit, suggesting conservation of relevant interactions in other evolutionary branches. Further mutagenesis experiments indicated that mutations at this site in ϵ -containing GABA_A receptors can change the apparent affinity of the agonist response to GABA, suggesting a potential role of this site in channel gating. In conclusion, this work details type-specific lipid interactions, which adds to our growing understanding of how lipids modulate pLGICs.

Pentameric ligand-gated ion channels (pLGICs) comprise a superfamily of membrane proteins known for their characteristic roles in fast synaptic transmission in the central and peripheral nervous systems. Elucidating the relationship of

these protein structures to their function has been of interest for several decades. In recent years, several atomic resolution structures from the pLGIC superfamily have been solved, and this includes members of the nicotinic acetylcholine receptors (nAChR) (1–4), serotonin-3 (5-HT₃) receptors (5–7), glycine receptors (8, 9), GABA_A receptors (10–15), the glutamate-gated chloride channel from *C. elegans*, GluCl (16, 17), and the prokaryotic channels ELIC (18) and GLIC (19, 20). Together, these structures provide a sagacious avenue for the development of new therapeutics.

The common architectural fold observed in these structures consists of a pentameric assembly of either identical (homopentamers) or nonidentical (heteropentamers) subunits each containing an extracellular domain (ECD), formed by an arrangement of β -strands connected *via* loops, followed by a transmembrane domain (TMD) comprised of four membrane-spanning helices (M1–M4) and an intracellular domain (ICD), which is formed by the loop connecting M3 and M4. The channel pore is lined by M2, allowing for the selective flux of permeant ions in the open conformation of the channel. The structural elucidation of representative members of this ion channel superfamily in different conformations has provided invaluable insight into the conformational changes of these channels during gating, but the role of the pore-forming transmembrane domain interactions with the membrane environment has been little explored (21–24).

In the past, lipids were thought to mainly serve as a structural scaffold for protein stability with occasional molecules bound, but as our knowledge of integral membrane proteins increases, so does our appreciation for the allosteric effects imparted by their immediate lipidic environments. Integral membrane proteins, including pLGICs, are organized into a specific three-dimensional structure that is governed in part by the energies associated with harmonizing the orientations of hydrophobic and hydrophilic residues with that of the host lipid matrix. It is well understood that to achieve the most energetically stable state, the length of the membrane-spanning domain containing hydrophobic residues should complement the thickness of the hydrophobic part of the lipid bilayer. This dynamic is believed to play a role in determining

[‡] These authors contributed equally to this work.

* For correspondence: Chris Ulens, chris.ulens@kuleuven.be; Rebecca J. Howard, rebecca.howard@scilifelab.se.

the organization of integral membrane proteins within the membrane (25–27).

Further insight into the functional role of lipids comes from studies on G-protein-coupled receptors (GPCRs), where negatively charged lipids enhance receptor activation in the absence of a bilayer and in a dose-dependent manner (28) or where linker residues mediate interactions with membrane-bound cholesterol (29). More generally, evidence suggests that lipids are not just a silent surrounding for membrane proteins but also represent key factors that can influence the expression and function of different classes of membrane proteins, including ion channels, aquaporins, GPCRs, transporters, and pumps (30–33). Of particular importance in these proteins are aromatic residues, which can interact with lipid headgroups, and in this study, we focused our attention on a Trp residue flanking the top of the M1-helix in the transmembrane domain of ELIC, a model prokaryotic pLGIC. Using a combination of complementary techniques, we investigate the functional contribution of this Trp residue to channel gating. Employing unnatural amino acid mutagenesis and electrophysiological recordings, we demonstrate that the Trp residue is involved in a cation- π interaction, although its partner is not obvious from structural data. Together with the known ability of the Trp residue to interact with the polar head group of a detergent molecule, we investigate whether the Trp residue interacts with cationic or zwitterionic lipids using molecular dynamics simulations. Finally, we extrapolate these findings to GABA_A receptors containing a conserved aromatic residue at this position. Together, our work sheds new light on lipid interactions in certain pLGICs.

Results

Residue W206 at the outward face of the ELIC transmembrane domain is involved in a cation- π interaction

To investigate the functional importance of tryptophan residues in the gating of ELIC, we focused on residue W206, which is near the boundary between the extracellular ligand-binding domain and the pore-forming transmembrane domain. This site at the top of the M1-helix forms part of the outward face of the ELIC transmembrane domain, which contacts the lipid bilayer. In ELIC, the W206 side chain points outward and into the lipid bilayer, potentially forming interactions with lipids. Our recently published ELIC structure (bound to a nanobody at a resolution of 2.5 Å) revealed new details of interacting ions, lipids, and detergent molecules (22). In this structure, W206 interacts with an undecylmaltoside molecule, with the W206 side chain pointing toward the polar head group and the lipophilic tail pointing downward along the M1-helix (Fig. 1A). Notably, this site has homologous topology to the ivermectin-binding site in the glutamate-gated chloride channel from *C. elegans* (Fig. 1B, pdb accession code 3rif) (16) and a POPC lipid-binding site in the $\alpha 1\beta 3\gamma 2$ GABA_AR structure (Fig. 1C, pdb accession code 6i53) (13). These observations raised the question as to whether the W206 in ELIC could also interact with lipid molecules in the context of the native lipid bilayer. Strikingly, an aromatic residue at this position is conserved in

selected eukaryotic receptors (Fig. 1D), including a putative 5-HT₃R in *C. latens*, the GABA_AR ϵ subunit in *Homo sapiens*, different insect GABA_AR subunits (*Papilio machaon*, *Heliothes viricens*, *Aedes aegypti*), nAChR subunits from coral (*Acropora digitifera*, *Acropora millepora* and *Stylophora pistillata*), the histamine-gated chloride channel from *Drosophila*, and various nAChR subunits from *Drosophila* and *Apis mellifera*. This conservation of an aromatic residue suggests a structural or functional role in these receptors.

To examine the contribution of W206 in this interaction, we investigated wild-type (WT) and mutant ELIC, transfected them into HEK293 cells, and probed GABA-elicited responses in a FlexStation using membrane potential sensitive dye (Fig. 2, A and B). Concentration–response curves for WT receptors revealed a GABA EC₅₀-value of 1.1 mM (pEC₅₀ = 2.96 ± 0.20) and a Hill coefficient of 2.2 ± 1.4, consistent with previously published data (34). Alanine substitution of W206 resulted in nonfunctional receptors (no response with up to 100 mM GABA), but we observed robust responses in receptors with W206Y (EC₅₀ 5.3 mM, pEC₅₀ = 2.272 ± 0.18, n = 4) and W206F mutations (EC₅₀ 2.0 mM, pEC₅₀ = 2.694 ± 0.08, n = 4). EC₅₀-values of these receptors were increased compared with WT ($p = 0.0008$), and for W206Y-containing receptors, maximal responses were smaller ($p = 0.0013$), likely indicating decreased expression. To determine if the π ring contributes to the interaction of W206, we substituted fluorinated Trp residues using noncanonical mutagenesis followed by two-electrode voltage clamp of receptors expressed in oocytes (Fig. 2C). All the fluorinated Trps resulted in increased EC₅₀-values, and plotting relative EC₅₀s against cation- π binding energy demonstrated a good correlation ($r^2 = 0.98$, Fig. 2D) indicating that such an interaction is important here for the function of the receptor. However, as no protein partner is apparent from the structure, these data indicate that a molecule in the membrane, most likely a lipid head group, contributes to this interaction.

An aromatic lipid-binding site at the outward complementary face of the ELIC transmembrane domain

To identify the specific lipid interactions contributing to the observed role of the W206 residue, we first performed triplicate 10- μ s molecular dynamics simulations using the coarse-grained MARTINI model (35). To differentiate on the basis of charge, a test membrane containing 20% anionic palmitoyloleoylphosphatidylglycerol (POPG) and 80% zwitterionic palmitoyloleoylphosphatidylcholine (POPC) lipids in each leaflet was simulated around the restrained protein. Consistent with previous reports (23), preferential interactions of POPG were observed in the inner leaflet, involving a cluster of basic residues on the inward-facing M3–M4 loop (Fig. 3, A and B). The more prevalent POPC was involved in a larger number of interactions, partly at the inward-facing M3–M4 site, but also an outward-facing site at the junction of the extracellular and transmembrane domains, involving the pre-M1 motif and upper M1 helix including residue W206- as well as proximal sites in upper M3 and M4 (Fig. 3, C and D).

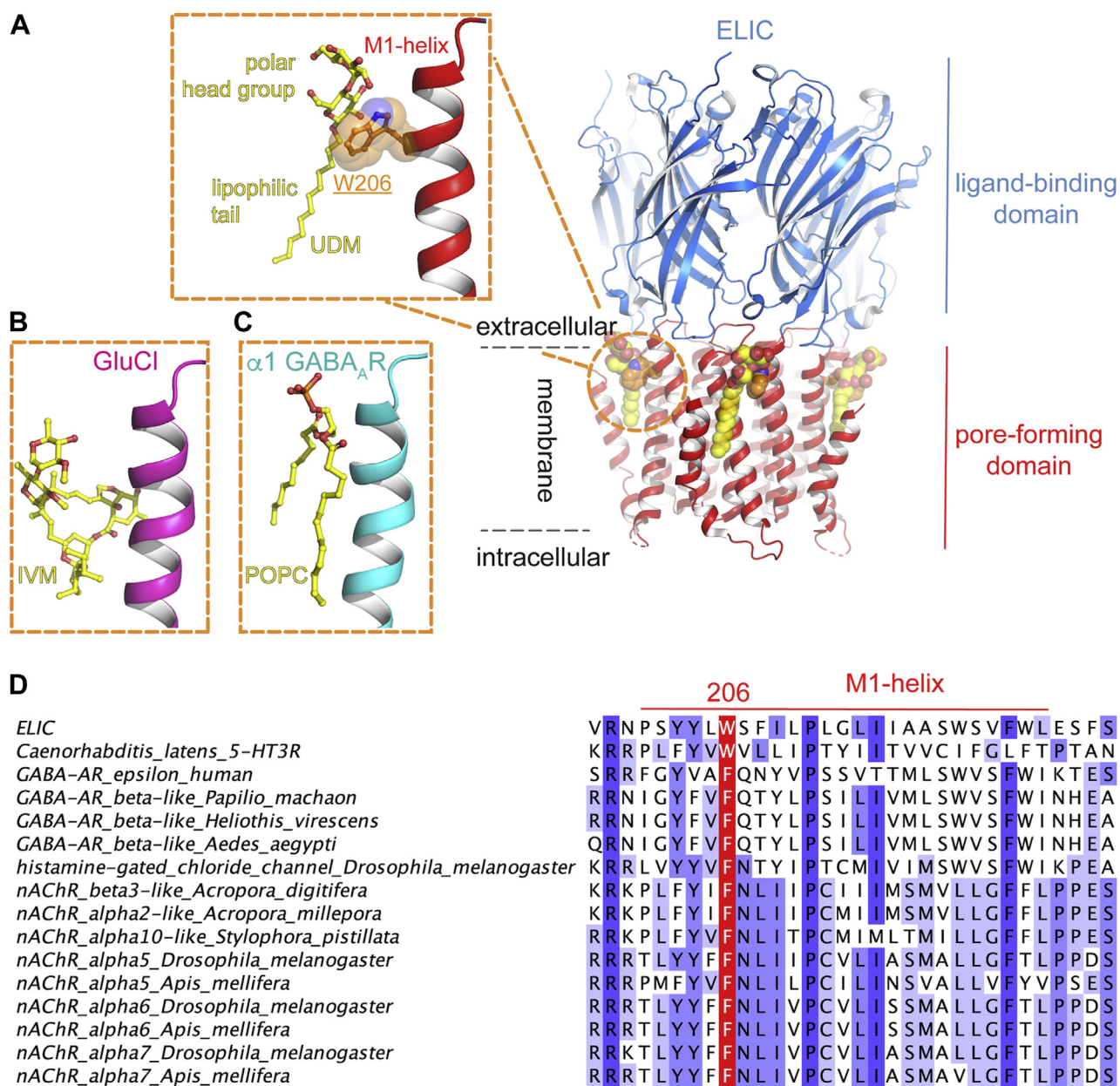


Figure 1. Location of a binding site for lipids, detergents, and lipophilic drugs at the outward transmembrane face of the pentameric ligand-gated ion channel ELIC. A, ELIC is shown in cartoon presentation with the extracellular ligand-binding domain shown in blue and the pore-forming transmembrane domain in red. The putative lipid binding is located near W206, shown as orange sticks, in the M1-helix. In a recently published 2.5 Å ELIC structure (pdb accession code 6hjx) (22), this site is occupied by a detergent molecule (undecylmaltoside), shown in yellow spheres. The inset shows a detail of the interaction, with the polar head group forming an interaction with W206. B, this binding site is homologous to the ivermectin (IVM, shown in yellow sticks) binding site in the glutamate-gated chloride channel from *C. elegans*, GluCl (pdb accession code 3rif) (16) and (C) a POPC (yellow sticks) binding site in the $\alpha 1\beta 3\gamma 2$ GABA_AR structure (pdb accession code 6i53) (13). D, sequence alignment showing conservation of aromatic residues (colored in red) at the position homologous to W206 in ELIC. Residues are colored in shades of blue by using an identity threshold of 20%.

We further investigated the structural basis for specific interactions in this putative outer-leaflet lipid site using unrestrained all-atom molecular dynamics simulations. As a starting model, ELIC was backmapped to atomistic resolution along with a representative POPC molecule at each of the five putative W206 sites. In triplicate simulations launched from this configuration, targeted POPC molecules were relatively stable, with the middle 50% equal to between 4 and 7 Å root-mean-squared deviation (RMSD) from the starting pose (Fig. 4A). Moreover, POPC headgroups distributed with a

median distance < 6 Å from the W206 sidechain, characteristic of a cation- π interaction (Fig. 4B) (36). In contrast, substituting alanine for the central tryptophan (W206A) allowed the lipid to deviate more widely, with the middle 50% between 5 and 10 Å in RMSD (Fig. 4A) and occupying a spread of positions centered > 8 Å from the mutated residue (Fig. 4B). Thus, W206 appeared to be important in retaining POPC at the outer-leaflet site. To test the charge dependence of this apparent interaction, we also ran atomistic simulations with the cationic lipid 1,2-dipalmitoyl-3-trimethylammonium-

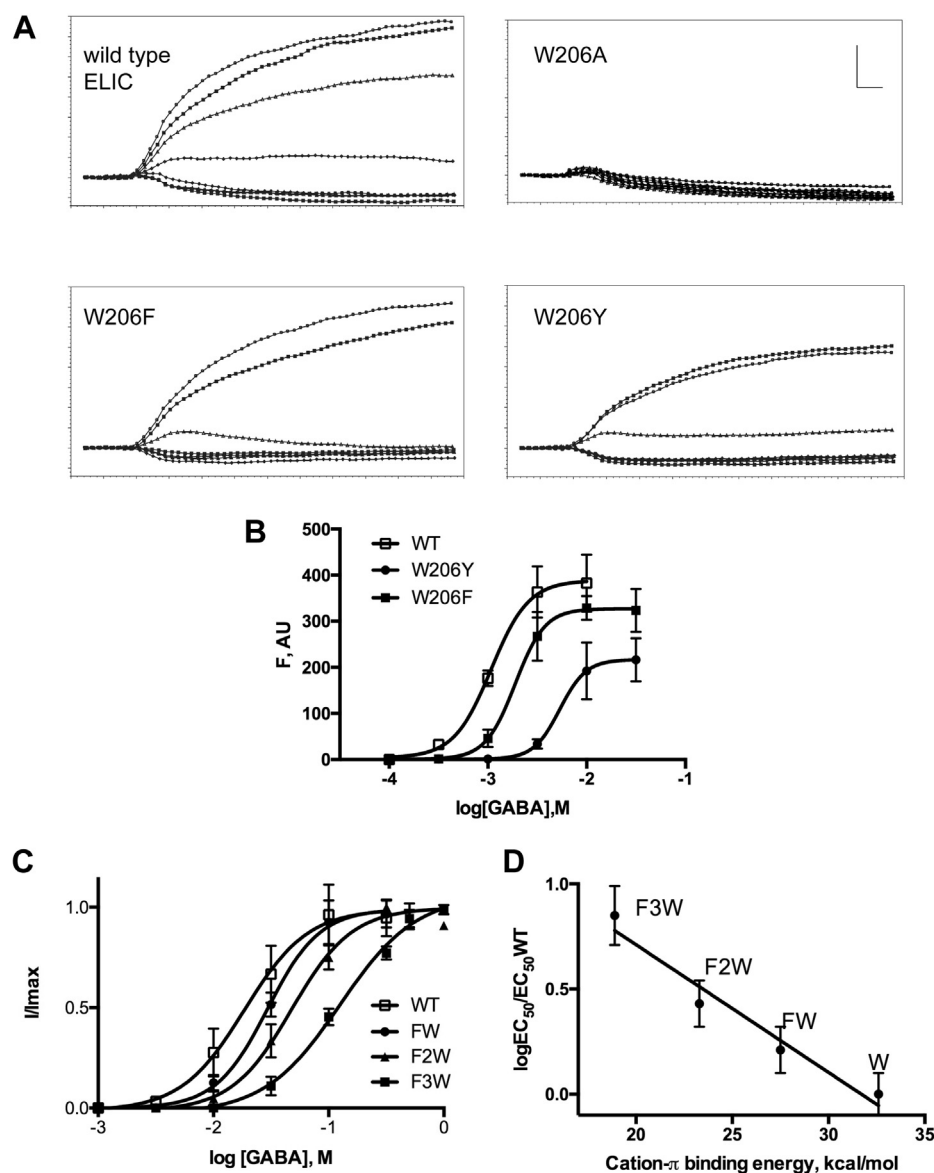


Figure 2. Functional characterization of W206 in ELIC through natural and noncanonical amino acid mutagenesis. *A*, typical FlexStation responses to application of GABA (0, 0.1, 0.3, 1, 3, 10, and 30 mM) at 20 s to HEK293 cells transfected with wild-type and mutant ELIC. Scale bar = 100 F, AU (arbitrary units) and 10 s. *B*, concentration–response curves from FlexStation data (mean \pm SD, $n = 4$). EC₅₀-values of these receptors were increased compared with wild-type ($p = 0.0008$), and for W206Y-containing receptors, maximal responses were smaller ($p = 0.0013$). Wild-type and mutant responses were compared using an ANOVA test followed by Dunnett’s multiple comparison test. *C*, concentration–response curves for ELIC assayed in oocytes showing the effects of incorporation of the noncanonical amino acids FW, F2W, and F3W at position 206 (mean \pm SD, $n = 4$). *D*, fluorination plot of W206 in ELIC. EC₅₀-values for ELIC activation by the agonist GABA in wild type (WT) and 1-F, 2-F, and 3-F substituted W206 are indicated as FW, F2W, and F3W, respectively. The plot of the EC₅₀-values relative to the cation- π binding energy reveals a linear correlation ($r^2 = 0.98$), which is indicative of a strong cation- π interaction with W206 in ELIC.

propane (DOTAP) or anionic POPG in place of zwitterionic POPC at each interface. Whereas behavior of DOTAP was markedly similar to POPC, anionic POPG deviated further from its starting position (Fig. 4*A*) and occupied a broad range of distances centered >9 Å from W206 (Fig. 4*B*), consistent with cation dependence.

Polar lipid contacts on the principal subunit

To elucidate structural determinants of lipid binding in the upper-leaflet site, we also probed contacts on the principal neighboring subunit (Fig. 5). Atomistic simulations revealed

prolonged interactions of M3-Q264 and M4-R318 with lipid-headgroup ester linkages (Fig. 5, *A–D*). Q264 was previously seen to coordinate detergent molecules bound at W206 (22); a role for R318 was less definitive, as this residue is not well resolved in many reported structures and was modeled *ab initio* for MD simulations. Moreover, removal of the M4 arginine side chain (R318A) was previously shown to enhance rather than diminish channel activity (37); indeed, ELIC has been shown to retain channel activity even upon deletion of M4 (22), suggesting that the M4–lipid interaction is not critical to function. To test the relevance of these apparent contacts, we ran additional simulations in the presence of DOTAP

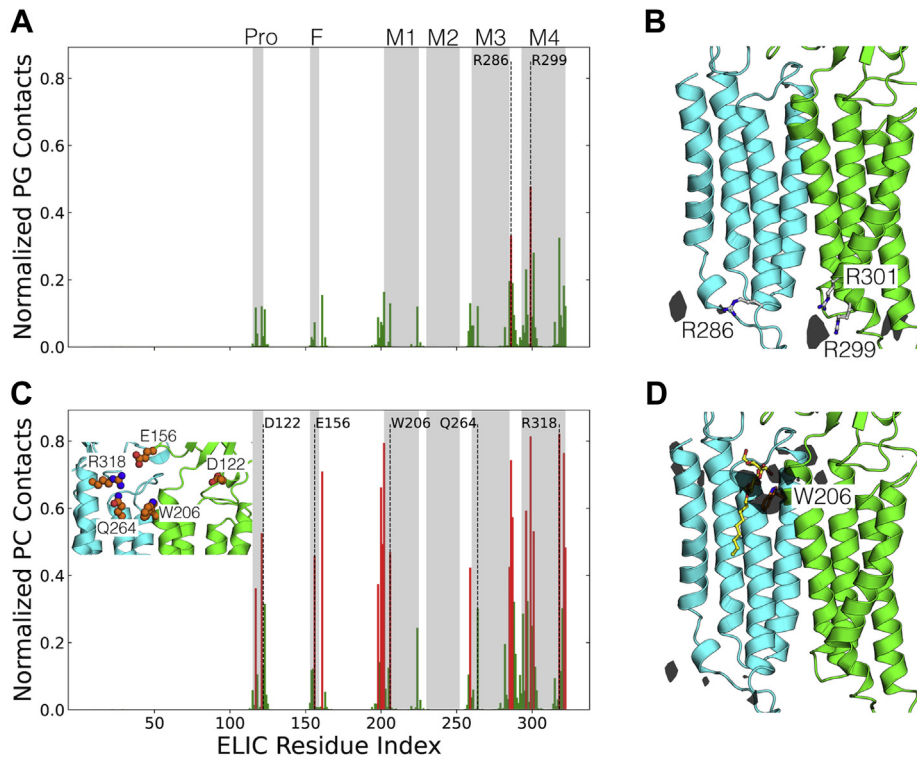


Figure 3. MD simulations with POPG and POPE lipids. A and C, normalized number of contacts between ELIC residues and headgroups of the POPG/POPE lipids from coarse-grained simulations. A contact was assumed if a residue's bead was within 5.5 Å of the lipid headgroup's bead and the contacts were subsequently averaged across the five subunits. Residues with a contact frequency of >33% are colored red. Residue indices corresponding to structural elements are highlighted in gray and important residues within them are highlighted and illustrated in the inset. B and D, densities of the different PG/PE lipids calculated from CG simulations illustrated at one of the subunit interfaces at an isosurface value of 1.9 molecules/nm³ and 5.0 molecules/nm³, respectively. For POPG, the R286, R299, and R301 residues mediating interactions with the anionic lipid are illustrated. For POPE, the M1-helix W206 residue adjacent to the preferential residence site is illustrated. Additionally, the detergent molecule identified to bind at this site in the PDB structure 6hix is overlaid on the subunit interface and illustrated in yellow.

with removal of the M3-glutamine side chain (Q264A), the entire M4 helix (Δ M4), or both features (Fig. 6). Either Q264A or Δ M4 allowed the lipid to deviate further from its starting

pose than in the WT system, and their combined effect was greater than either individual modification (Fig. 6A). Moreover, analysis of choline-W206 distances indicated

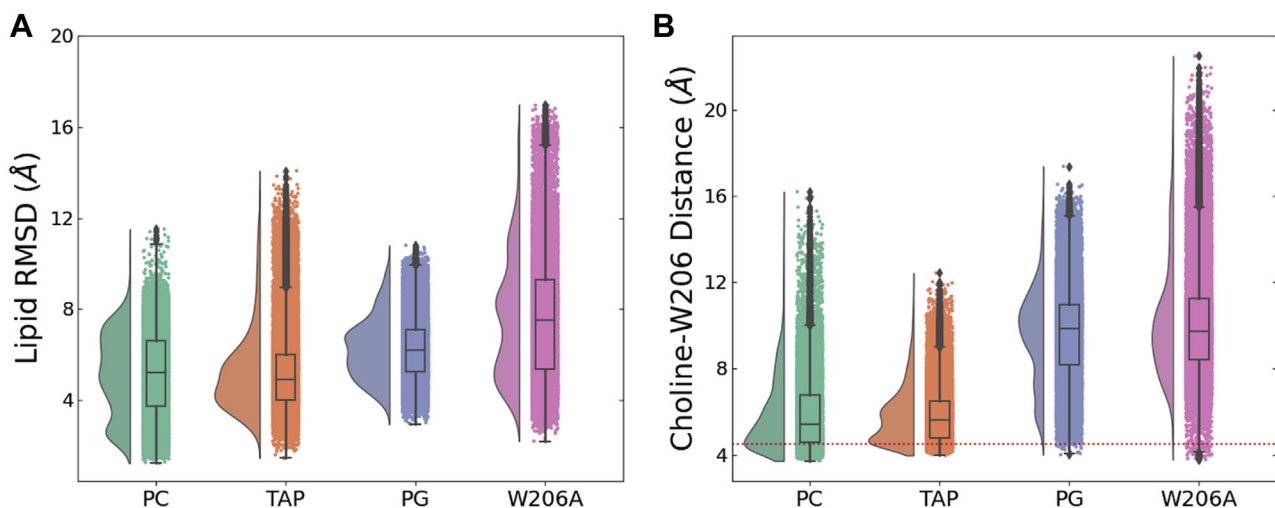


Figure 4. Stability of different lipids at the W206-binding site. A, stability of various lipid types at the intersubunit binding site illustrated by the RMSD probability distributions and box plots. For this calculation, the C α atoms of the M2 helix were first aligned and the RMSD was calculated for the non-hydrogen lipid headgroup atoms. The RMSD values were then averaged across the five subunit interfaces over the final 150 ns of three independent 300 ns MD trajectories. B, the role of cation- π interactions in stabilizing the lipid at the subunit interface illustrated by the distribution of distance between the choline lipid headgroup and the center of the W206 aromatic side chain. For each lipid type, the distances were averaged across the five subunit interfaces over the final 150 ns of three independent 300 ns MD trajectories. For the PG lipid without the choline group, the distances were instead calculated to the phosphorus atom and the ideal cation- π binding distance of 4.5 Å is illustrated as a dotted red line. Data are presented as a box plot

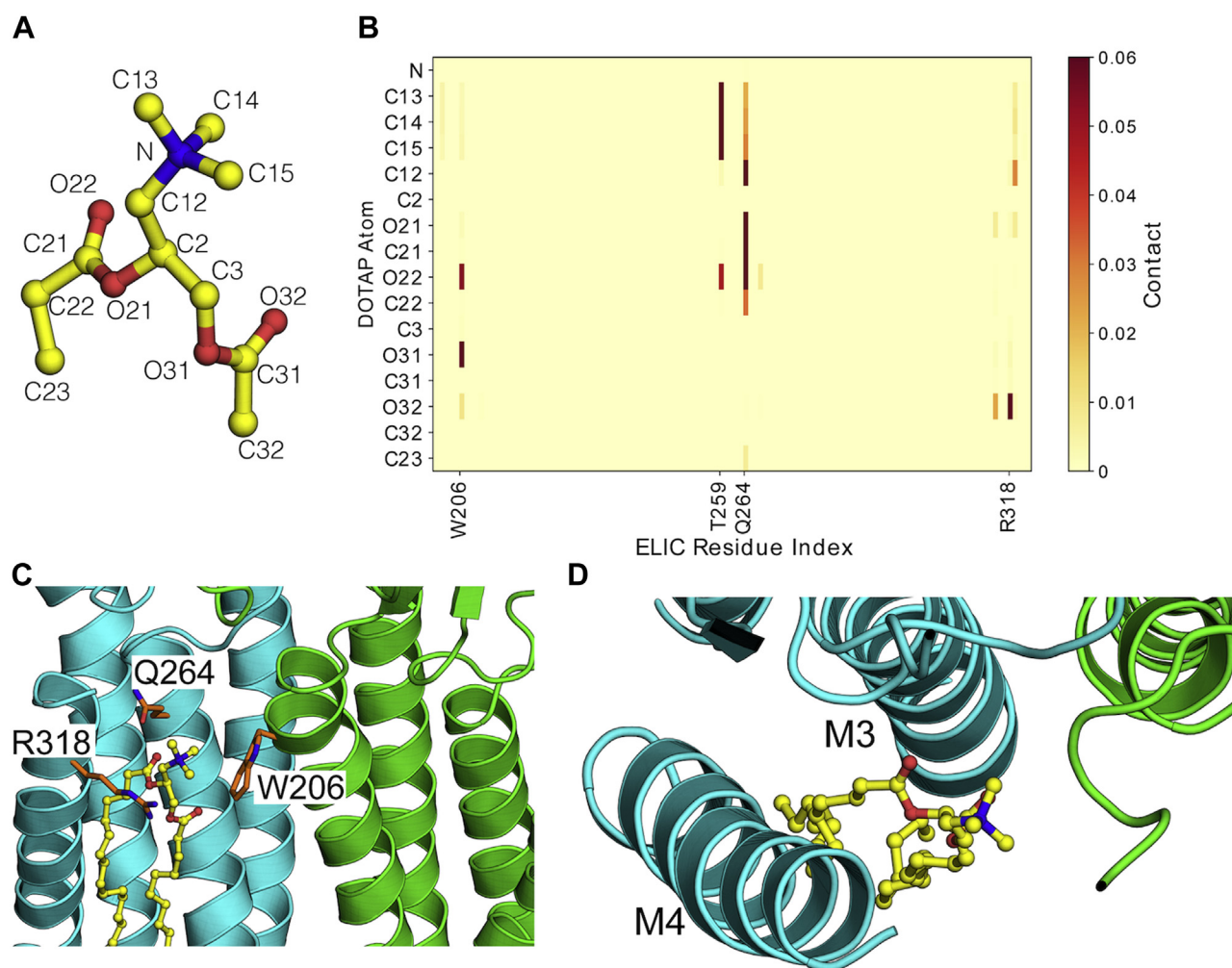


Figure 5. Amino acid interactions of lipid bound at the intersubunit-binding site. A and B, secondary contacts stabilizing the lipid at the intersubunit binding site illustrated as a contact map with the headgroup of the cationic DOTAP lipid. A contact was assumed if a nonhydrogen atom of the residue was within 3.2 Å of the lipid atom. The contacts are averaged across the five subunit interfaces over the final 150 ns of three independent 300 ns MD trajectories. C, the W206, Q264, and R318 side chains are illustrated in orange relative to the position of the lipid (in yellow) at the subunit interface. D, top view of the transmembrane domain shows how the lipid (in yellow) couples the M3/M4 helices, possibly influencing gating.

considerable dissociation of this cation- π interaction in the presence of Q264A, with or without M4 (Fig. 6B). Thus, polar contacts in M3 and possibly M4 appeared to directly support cation- π lipid interactions with the complementary M1-helix.

Site-directed mutagenesis of M1 aromatic residue in $\alpha 1\beta 2\epsilon$ GABA_AR expressed in *Xenopus oocytes*

To verify the importance of an aromatic residue at the top of the M1-helix in eukaryotic receptors, we mutated the homologous residue in the GABA_AR ϵ -subunit, F260 (numbering according to mature protein). Using two electrode voltage clamp recordings from *Xenopus oocytes* expressing WT and mutant receptors, comprising ϵ plus $\alpha 1$ and $\beta 1$ subunits, we then determined EC₅₀-values in response to the agonist GABA. Substitution of a nonaromatic glutamic acid residue (ϵ F260E) decreased apparent GABA affinity threefold (Fig. 7): GABA EC₅₀-values were 2.27 ± 0.60 (n = 6, WT) and 6.52 ± 1.80 (n = 12, ϵ F260E). A *t* test indicates a *p*-value of $<2.5 \times 10^{-6}$. This disruptive effect was consistent with a direct or

indirect role of F260 in gating of ϵ -containing GABA_ARs, possibly involving lipid modulation, although insignificant effects of other substitutions (F260I, F260R) may indicate compensatory or complex interactions at this site.

Discussion

An increasing number of structural and biophysical studies have revealed lipid interactions in different classes of membrane proteins, including ion channels and GPCRs, which are important drug targets (reviewed in (38–40)). A crucial role in identifying some of these lipid interactions has been provided by molecular dynamic simulations (38, 39), through complementation of experimental structural studies, such as X-ray crystallography or cryo-EM, which often reveal electron densities that do not permit an unambiguous assignment of the lipid identity. Membrane-lipid interactions were originally thought to primarily maintain structural integrity, but it is becoming increasingly clear that lipids also have other roles, including as cofactors and in influencing protein activity, and

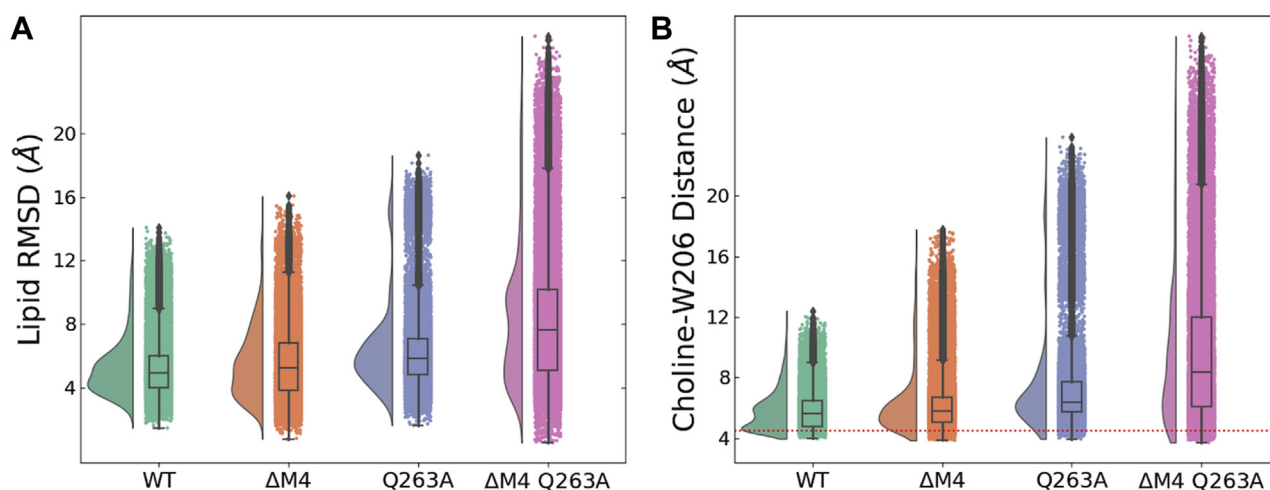


Figure 6. Role of M2 and M4 polar contacts in lipid interactions. *A*, the role of the M2 and M4 polar contacts in stabilizing the lipid at the subunit interface analyzed by lipid RMSD probability distributions and box plots. For this calculation, the C α atoms of the M2-helix were first aligned and the RMSD was calculated for the nonhydrogen DOTAP headgroup atoms. The RMSD values were then averaged across the five subunit interfaces over the final 150 ns of three independent 300 ns MD trajectories. *B*, the role of the M2- and M4-helix polar contacts in stabilizing the lipid at the subunit interface analyzed by the distribution of the DOTAP Choline-W206 side chain distance. The distances were averaged across the five subunit interfaces over the final 150 ns of three independent 300 ns MD trajectories. The ideal cation- π binding distance of 4.5 Å is illustrated as a dotted red line. Data are presented as a box plot.

may in fact be central to biological function (41). Lipids can also affect protein trafficking, with the best studied example relevant to our work being palmitoylation of nACh and GABA_A receptors, which has a dramatic effect on membrane expression levels and, for GABA_AR, is essential for synaptic localization (42, 43). We do not observe palmitoylation here, and although our data showing a lower maximal response (~60% of WT, Fig. 2) in W206Y ELIC suggest that altering lipid-binding sites may have the potential to alter expression levels, the fivefold increase in EC₅₀ indicates a definite effect on receptor activity; thus we have not (yet) explored lipid-modulated expression further, but in this study have concentrated on probing lipid effects on protein function.

It is of course possible that W206 mediates activation by a mechanism that does not involve lipids, but we observed no extensive interactions of this residue with any other protein elements and certainly not with any cationic groups capable of explaining the noncanonical amino acid effects. Conversely, we do see substantial, specific interactions with zwitterionic or cationic lipids capable of cation- π binding, with plausible coupling to other regions associated with gating (M3/M4). We do appreciate that there are some limitations to our simulations in that our initial structure was a nonconducting, possibly decoupled, receptor, and it is not yet clear if this best resembles a resting, active, or desensitized state (or none of these). We also do not know exactly which cation-containing lipid species predominate in *D. didantii* and so used POPC as a lipidic example as it is relatively well characterized for simulations. Many lipids (and especially PC) can of course act as solvents for membrane proteins, and even the identification of a specific lipid-binding site does not necessarily imply functional relevance, hence the importance of experimental data such as we have provided here. Thus overall our combined computational and experimental data strongly support our hypothesis that a lipid-protein cation- π interaction

facilitates activation coupling, and this could be disrupted by mutations, as well as by lipophilic modulators, and perhaps also by dynamic regulation of the relevant lipid species.

One of the best-described examples of protein modulation by lipids comes from the class of inwardly rectifying K⁺ (Kir) channels, which are activated by the anionic phospholipid PIP2 (phosphatidylinositol 4,5-bisphosphate) (44). The PIP2 interaction site has been observed in several Kir structures, including Kir2 (45), and involves highly conserved basic residues (arginine and lysine) from the TM helices and cytoplasmic domain that interact with the negatively charged PIP2. Combined electrophysiological studies and MD simulations have revealed the dynamic nature of the PIP2 interaction (46), which involves a stabilization of the interaction between the TM domain and the cytoplasmic domain, thereby opening the channel gate.

In the related class of voltage-gated (Kv) K⁺ channels, a phosphatidylglycerol (PG) lipid has been observed in the crystal structure of a Kv1.2/Kv2.1 chimeric channel. Here, the lipid wedges between the S1-S4 voltage-sensor domain (VSD) and the S5-S6 pore domain, thereby coupling voltage-sensor motions to pore opening (47). A combination of MD simulations (48) and functional studies (49) has indeed confirmed the phospholipid interactions with arginines in the voltage sensor and indicated that phospholipids facilitate voltage-driven conformational transitions, thereby enabling lipid-dependent gating of Kv channels (50).

These two examples suggest ways by which lipids might alter the function of ELIC, *i.e.*, by modulating interactions within the protein that control channel kinetics or by facilitating agonist-gated conformational change. Evidence to support the former hypothesis comes from studies in a range of pLGICs, which have demonstrated the role in lipids *via* the outermost, lipid contacting, M4-helix (21, 22). Of particular relevance to this work, in a recent study on ELIC, we

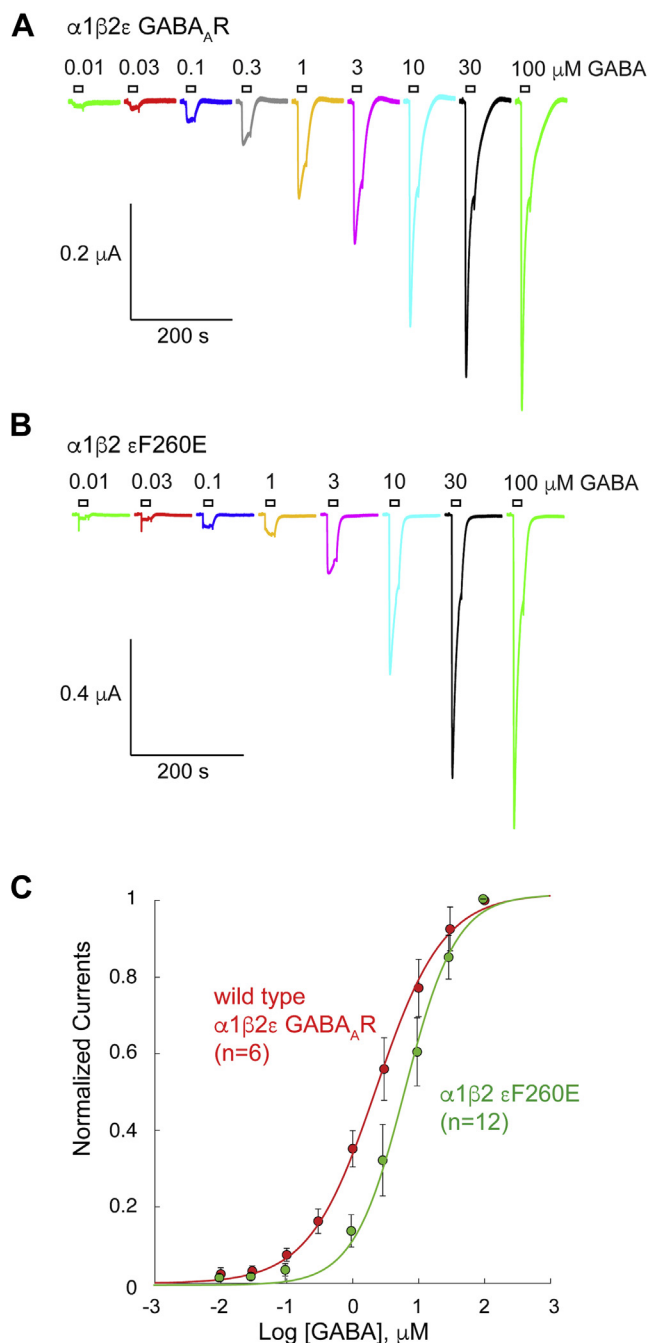


Figure 7. Functional characterization of the epsilon-F260E mutant in *Xenopus* oocytes. A and B, representative current traces evoked from *Xenopus* oocytes expressing the wild-type human $\alpha 1\beta 2\epsilon$ GABA_AR (A) and the $\alpha 1\beta 2\epsilon$ F260E mutant (B). Agonist-evoked currents were obtained by application of the GABA concentrations as indicated. C, concentration-response relationships for the experiments indicated in A and B. GABA EC₅₀-values were 2.27 ± 0.60 (n = 6, wild type) and 6.52 ± 1.80 (n = 12, ϵ F260E). An unpaired, two-tailed t test with Welch's correction gave a p-value of $<2.5 \times 10^{-6}$. Data are presented as mean \pm SD.

demonstrated that a phosphatidylethanolamine (PE) lipid binds at the lower half of the M1- and M4-helices and to M3, overlapping a known binding site for neurosteroids (51–53), cholesterol (11), and general anesthetics (54). This site is shaped by a characteristic proline-kink halfway the M4-helix, which is conserved in eukaryotic GABA_A and glycine

receptors. Using a combination of complementary methods, we demonstrated that M4 is intrinsically flexible and that M4 deletions or mutations of the lipid-binding site accelerate desensitization, a phenomenon that can be mimicked by reconstitution of ELIC into membranes of different lipid composition (22). These data indicate that M4 acts as a lipid sensor and that lipid interactions shape the agonist response. Further evidence into the role of the M4-helix comes from studies on the *Torpedo* nAChR, which revealed that in the absence of anionic lipids and cholesterol, the receptor binds agonist, but does not undergo agonist-induced conformational transitions, a phenomenon that has been called receptor “uncoupling” (21).

In addition to the lipid-binding site at the lower half of the M4-helix, several other lipid-binding sites have been resolved in pLGICs. A detailed review of each of those individual lipid sites would be beyond the scope of this discussion, but as an example in GLIC, two phosphatidylcholine (PC)-binding sites are located in a groove between M4 and both M1 and M3 (19), one in the upper half and the other in the lower half of the TM domain. The lipid bound in the upper half of the TM domain is displaced in the GLIC structure bound to the general anaesthetic propofol (54).

As an example in eukaryotic receptor structures, a cryo-EM structure of the full-length $\alpha 1\beta 3\gamma 2$ GABA_AR in lipid nanodiscs revealed PIP2 molecules bound to the intracellular side of the TM domain, forming polar interactions between the PIP2 phosphate headgroup and basic (arginine and lysine) side chains of the $\alpha 1$ M3 and M4 helices (13). In a recent cryo-EM structure of the $\alpha 4\beta 2$ nAChR, two cholesterol molecules per receptor subunit were bound at the receptor periphery along the intracellular half of the transmembrane domain and flanking the subunit interface (2).

Within the context of the present study, which focuses on a lipid-binding site at the top of the M1-helix (W206 in ELIC), it is worth discussing several other studies that have revealed lipids or lipophilic compounds bound at or near to this site in different pLGICs. For example, in the glutamate-gated chloride channel from *C. elegans* (pdb code 3rif) (16), the allosteric agonist ivermectin is bound to the same site, forming interactions with L218 (equivalent to W206) and V278 (equivalent to Q264). In the $\alpha 1\beta 3\gamma 2$ GABA_AR structure (pdb code 6i53) (13), POPC is in contact with $\alpha 1$ -I228 (equivalent to W206) and $\beta 3$ -M283 (equivalent to Q264), although the lipid is somewhat excluded from the cleft. In $\alpha 1\beta 2\gamma 2$ GABA_AR structures (pdb codes 6x3x, 6x3t) (15), weak putative lipid densities are intercalated at $\alpha 1/\beta 2$ and $\alpha 1/\gamma 2$ interfaces, potentially proximal to $\beta 2$ -L223/ $\gamma 2$ -I238 (equivalent to W206) and/or $\alpha 1$ -W288 (equivalent to Q264), although lack of resolution precludes identifying direct contacts. In 6x3t, propofol is resolved at $\beta 2/\alpha 1$ interfaces, deeper than ELIC lipids but still in contact with the backbone of $\alpha 1$ -I228 (equivalent to W206) and enabling visualization of additional putative lipid densities at the interface periphery. Taken together, these studies demonstrate that the W206 site at the top of the M1-helix in ELIC is structurally equivalent in different pLGICs and can serve as a binding site for lipids or lipophilic drugs.

In summary, our study investigates the outward transmembrane face in ELIC as a lipid-binding site. Using a combination of complementary methods, we investigated the role of W206 in lipid interactions. Using noncanonical mutagenesis, we reveal that W206 is involved in a cation- π interaction. Together with previous structural data showing that the W206 engages in interactions with the polar headgroup of a detergent molecule, we investigated interactions of W206 with cationic and zwitterionic lipids using molecular dynamics simulations. Using site-directed mutagenesis, we show that the conserved aromatic residue in the GABA_AR ϵ -subunit affects gating and speculate that this is due to modulating interactions within the protein that control channel kinetics. Together, these results expand our knowledge of lipid interaction sites in pLGICs.

Experimental procedures

FlexStation methods

These methods were similar to those previously described (55). Briefly, ELIC cDNA was transfected into HEK293 cells, and these were then grown for 2 to 3 days in a 96-well plate. Then blue fluorescent membrane potential dye (Molecular Devices Ltd) diluted in Flex buffer (10 mM HEPES, 115 mM NaCl, 1 mM KCl, 1 mM CaCl₂, 1 mM MgCl₂, 10 mM glucose, pH 7.4) was added to each well. After incubation at 37 °C for 30 min, plates were placed in a FlexStation (Molecular Devices Ltd) and fluorescence measured every 2 s for 120 s. Buffer or GABA (0.03–30 mM) was added to each well after 20 s. Concentration–response data were fitted to the four-parameter logistic equation, $F = F_{\min} + (F_{\max} - F_{\min}) / (1 + 10^{\log(EC_{50} - [A]) * nH})$, where [A] is the concentration of agonist, nH is the Hill coefficient, and F_{\max} and F_{\min} are the maximal and minimal fluorescence levels for each dataset, using Prism software (GraphPad). WT and mutant responses were compared using an ANOVA test followed by Dunnett's multiple comparison test.

Noncanonical amino acid incorporation

Site-directed mutagenesis was performed using the QuikChange strategy (Stratagene) using ELIC in pGEM-HE. Mutations were confirmed by sequencing. For noncanonical amino acid mutants, the site of interest was mutated to the TAG stop codon. Plasmids were linearized and receptor mRNA prepared by *in vitro* runoff transcription using the Ambion T7 mMessage mMachine kit. Noncanonical amino acids ligated to tRNA were prepared as previously described (56).

Stage V–VI oocytes of *Xenopus laevis* were harvested and injected with mRNAs as described previously. For experiments with WT channels and conventional mutants, each cell received a single injection of 10 to 25 ng of receptor mRNA approximately 24 h before recording. For nonsense suppression experiments, each cell was injected with 50 to 100 ng each of receptor mRNA and appropriate tRNA approximately 48 h before recording. Injection volumes for each injection session were 50 to 100 nl per cell.

ELIC electrophysiology

Two-electrode voltage clamping of *Xenopus* oocytes was performed using an OpusXpress system (Axon Instruments, Inc). All experiments were performed at 22 to 25 °C. GABA (Sigma) was diluted in ND-96 and delivered to cells *via* a computer-controlled perfusion system. Glass microelectrodes were backfilled with 3 M KCl and had a resistance of approximately 1 M Ω . The holding potential was –60 mV unless otherwise specified. Concentration–response curves and parameters were obtained using Prism software (GraphPad, PRISM).

Model building

As a starting model for ELIC simulations, protein atoms from a 2.5-Å resolution X-ray structure (PDB ID 6HJX) (22) were extracted from their associated nanobodies, lipids, and detergent molecules. Unresolved residues at the M4 C-terminus of each subunit were built as a continuous helix using PyMOL. Since cation- π interactions due to the orbital orientations in aromatic rings are not treated explicitly in simulations, care was taken to use force fields with appropriate corrections for all models (57).

Coarse-grained simulations

Coarse-grained simulations were performed using the MARTINI 2.3P polarizable force field (35) with improved choline-aromatic cation- π interaction parameters (58). Each protein was embedded in a symmetric membrane containing 80% POPC and 20% POPG, or a brain–lipid mimic mixture as previously described (15), using the Martini Bilayer Maker (59) in CHARMM-GUI (60). The membrane spanned a dimension of 300 \times 300 Å containing 2180 lipids and 283,597 beads including ions and polarizable water (61). After energy minimization and equilibration for 20 ns, three replicates of each system were simulated for 10 μ s using GROMACS 2018 (62), with all protein beads restrained to allow convergence of lipid interactions.

The final 7.5 μ s of the simulation trajectories was used for analysis using Python MDAnalysis/MDTraj scripts (63, 64). A contact was assumed if a residue's bead was within 5.5 Å of a lipid head-group bead, and occupancy probability density calculations were performed using a 2 Å-resolution grid.

Atomistic simulations

As a starting model, ELIC was backmapped to atomistic resolution using Backward (65) along with a POPC molecule from a representative coarse-grained simulation frame, occupying the high-probability volume associated with a single receptor subunit. This lipid was then replicated and symmetrized to occupy each of the five putative sites in the pentameric channel. PyMOL (<http://www.pymol.org>) was used to introduce mutations at the lipid-binding site, and alternative lipids (DOTAP, POPG) were substituted by alignment of their head- and acetyl groups. The structure with five bound lipids was then placed in a POPC bilayer of dimension 150 \times 150 Å using CHARMM-GUI (60). The Charmm36M force field (66)

with WYF cation- π corrections (67) was used to describe the system in GROMACS using the nbfix settings, applying corrections to nonbonded contacts between all methylated ammonium and aromatic groups with no apparent impact on performance.

After equilibration, three replicates of each system were simulated for 300 ns using GROMACS 2018 (62) and a timestep of 2 fs. Long-range electrostatic interactions were calculated using the particle mesh Ewald method (68) and hydrogen-bond lengths were constrained using LINCS (69). Pressure and temperature were maintained through the use of the Parrinello–Rahman barostat (1 bar) (70) and v-rescale (300 K) thermostat (71), respectively. Lipid-binding stabilities were calculated as an average over all five subunit interfaces from the final 150 ns of all replicates.

GABA_A receptor electrophysiology

The sequence of the gene encoding the GABA_AR ϵ subunit corresponding to the accession number NM_004961 was synthesized by Blue Heron Biotech into the pCMV6-AC vector from Origen, which offers the advantage of allowing expression in eukaryotic cells with the cytomegalovirus (CMV) promoter as well as the bacterial T7 promoter for *in vitro* synthesis of mRNA. The nucleotide sequence was optimized for expression in mammalian cells using standard procedures. Mutations were engineered with a QuikChange strategy and confirmed by sequencing. For functional expression of GABA_AR containing an ϵ subunit, the mRNAs encoding for the human $\alpha 1$ (NP_000797.2), $\beta 2$ (NP_068711.1) and ϵ subunits were mixed in a 1:1:0.1 ratio in nuclease-free distilled water at a concentration of 0.4 $\mu\text{g}/\mu\text{l}$ (n.b. the definitive stoichiometry of the expressed receptors was not determined). Following standard preparation of the oocytes (72), stage V and VI cells were manually selected under a binocular and disposed in a 96 microtiter plate previously filled with ND96-solution containing 96 mM NaCl, 2 mM KCl, 1.8 mM CaCl₂, 2 mM MgCl₂ and 5 mM HEPES, pH 7.4, supplemented with 50 mg/l gentamicin sulfate. Injection of 2 ng of mRNA per oocyte was done using the automated injection system Roboinject (Multi Channel Systems). Oocytes were incubated at 18 °C for 2 to 5 days prior to conducting the electrophysiological recordings using the two electrode automated voltage clamp system (HiClamp apparatus, Multi Channel Systems). A standard OR2 solution containing 82.5 mM NaCl, 2.5 mM KCl, 1.8 mM CaCl₂, 1 mM MgCl₂, and 5 mM HEPES buffered at pH 7.4 was used as control and cells were maintained at 20 °C using the cooling system of the HiClamp. Currents were evoked by brief exposure to GABA as indicated in the figures. Data acquired with the HiClamp were analyzed using the manufacturer's software (Multi Channel Systems). Concentration-activation curves were fitted with the empirical Hill equation. Data are presented as the mean \pm standard deviation (SD). Statistical comparison between WT and mutants was done with an unpaired, two-tailed *t* test with Welch's correction for unequal sample size and variance.

Data availability

Sample frames from coarse-grained and atomistic MD trajectories are available on [zenodo.org](https://doi.org/10.5281/zenodo.4618338) with <https://doi.org/10.5281/zenodo.4618338>.

Acknowledgments—We thank DA Dougherty (Caltech, USA) for supplying the nonconventional amino acids and hosting those experiments. Computational resources were provided by the Swedish National Infrastructure for Computing (SNIC).

Author contributions—A. S., S. C. R. L., D. B., E. L., R. J. H., and C. U. conceptualization; A. S., S. C. R. L., K. K., D. B., and R. J. H. data curation; A. S., S. C. R. L., M. B., K. K., D. B., E. L., and R. J. H. formal analysis; S. C. R. L., E. L., and C. U. funding acquisition; A. S., S. C. R. L., M. B., K. K., D. B., E. L., and R. J. H. investigation; A. S., S. C. R. L., M. B., K. K., D. B., E. L., and R. J. H. methodology; A. S. software; R. J. H. and C. U. supervision; A. S., S. C. R. L., K. K., D. B., R. J. H., and C. U. visualization; A. S., S. C. R. L., D. P., A. M., M. B., K. K., D. B., E. L., R. J. H., and C. U. writing—original draft; R. J. H. and C. U. writing—review and editing.

Funding and additional information—A. S. was supported by Marie Skłodowska-Curie grant 898762, and E. L./R. J. H. by grants from the Swedish Research Council (2017-04641, 2019-02433) and Swedish e-Science Research Center. S. C. R. L. was supported by the MRC grant MR/L021676. C. U. was supported by grants from FWO-Vlaanderen (G0C9717N, G0C1319N) and KU Leuven (C3/19/023, C14/17/093).

Conflict of interest—The authors declare no conflict of interest.

Abbreviations—The abbreviations used are: DOTAP, dipalmitoyl-3-trimethylammonium-propane; ECD, extracellular domain; GPCR, G-protein-coupled receptor; ICD, intracellular domain; nAChR, nicotinic acetylcholine receptor; PC, phosphatidylcholine; PE, phosphatidylethanolamine; PG, phosphatidylglycerol; pLGIC, pentameric ligand-gated ion channel; POPC, palmitoyloleoylphosphatidylcholine; POPG, palmitoyloleoylphosphatidylglycerol; RMSD, root-mean-squared deviation; TMD, transmembrane domain; VSD, voltage-sensor domain; WT, wild-type.

References

1. Morales-Perez, C. L., Noviello, C. M., and Hibbs, R. E. (2016) X-ray structure of the human $\alpha 4\beta 2$ nicotinic receptor. *Nature* **538**, 411–415
2. Walsh, R. M., Roh, S.-H., Gharpure, A., Morales-Perez, C. L., Teng, J., and Hibbs, R. E. (2018) Structural principles of distinct assemblies of the human $\alpha 4\beta 2$ nicotinic receptor. *Nature* **557**, 261–265
3. Gharpure, A., Teng, J., Zhuang, Y., Noviello, C. M., Walsh, R. M., Cabuco, R., Howard, R. J., Zaveri, N. T., Lindahl, E., and Hibbs, R. E. (2019) Agonist selectivity and ion permeation in the $\alpha 3\beta 4$ ganglionic nicotinic receptor. *Neuron* **104**, 501–511.e6
4. Rahman, M. M., Teng, J., Worrell, B. T., Noviello, C. M., Lee, M., Karlin, A., Stowell, M. H. B., and Hibbs, R. E. (2020) Structure of the native muscle-type nicotinic receptor and inhibition by snake venom toxins. *Neuron* **106**, 952–962.e5
5. Hassaine, G., Deluz, C., Grasso, L., Wyss, R., Tol, M. B., Hovius, R., Graff, A., Stahlberg, H., Tomizaki, T., Desmyter, A., Moreau, C., Li, X.-D., Poitevin, F., Vogel, H., and Nury, H. (2014) X-ray structure of the mouse serotonin 5-HT₃ receptor. *Nature* **512**, 276–281
6. Basak, S., Gicheru, Y., Samanta, A., Molugu, S. K., Huang, W., la de Fuente, M., Hughes, T., Taylor, D. J., Nieman, M. T., Moiseenkova-Bell,

- V., and Chakrapani, S. (2018) Cryo-EM structure of 5-HT 3A receptor in its resting conformation. *Nat. Commun.* **9**, 514
7. Polovinkin, L., Hassaine, G., Perot, J., Neumann, E., Jensen, A. A., Lefebvre, S. N., Corringer, P.-J., Neyton, J., Chipot, C., Dehez, F., Schoehn, G., and Nury, H. (2018) Conformational transitions of the serotonin 5-HT₃ receptor. *Nature* **563**, 275–279
 8. Du, J., Lü, W., Wu, S., Cheng, Y., and Gouaux, E. (2015) Glycine receptor mechanism elucidated by electron cryo-microscopy. *Nature* **526**, 224–229
 9. Huang, X., Chen, H., Michelsen, K., Schneider, S., and Shaffer, P. L. (2015) Crystal structure of human glycine receptor- α 3 bound to antagonist strychnine. *Nature* **526**, 277–280
 10. Miller, P. S., and Aricescu, A. R. (2014) Crystal structure of a human GABAA receptor. *Nature* **512**, 270–275
 11. Zhu, S., Noviello, C. M., Teng, J., Walsh, R. M., Kim, J. J., and Hibbs, R. E. (2018) Structure of a human synaptic GABAA receptor. *Nature* **559**, 67–72
 12. Phulera, S., Zhu, H., Yu, J., Claxton, D. P., Yoder, N., Yoshioka, C., and Gouaux, E. (2018) Cryo-EM structure of the benzodiazepine-sensitive α 1 β 1 γ 2 δ tri-heteromeric GABAA receptor in complex with GABA. *Elife* **7**, e39383
 13. Laverty, D., Desai, R., Uchański, T., Masiulis, S., Stec, W. J., Malinauskas, T., Zivanov, J., Pardon, E., Steyaert, J., Miller, K. W., and Aricescu, A. R. (2019) Cryo-EM structure of the human α 1 β 3 γ 2 GABAA receptor in a lipid bilayer. *Nature* **565**, 516–520
 14. Masiulis, S., Desai, R., Uchański, T., Martin, I. S., Laverty, D., Karia, D., Malinauskas, T., Zivanov, J., Pardon, E., Kotecha, A., Steyaert, J., Miller, K. W., and Aricescu, A. R. (2019) GABAA receptor signalling mechanisms revealed by structural pharmacology. *Nature* **565**, 454–459
 15. Kim, J. J., Gharpure, A., Teng, J., Zhuang, Y., Howard, R. J., Zhu, S., Noviello, C. M., Walsh, R. M., Lindahl, E., and Hibbs, R. E. (2020) Shared structural mechanisms of general anaesthetics and benzodiazepines. *Nature* **585**, 303–308
 16. Hibbs, R. E., and Gouaux, E. (2011) Principles of activation and permeation in an anion-selective Cys-loop receptor. *Nature* **474**, 54–60
 17. Althoff, T., Hibbs, R. E., Banerjee, S., and Gouaux, E. (2014) X-ray structures of GluCl in apo states reveal a gating mechanism of Cys-loop receptors. *Nature* **512**, 333–337
 18. Hilf, R. J. C., and Dutzler, R. (2008) X-ray structure of a prokaryotic pentameric ligand-gated ion channel. *Nature* **452**, 375–379
 19. Bocquet, N., Nury, H., Baaden, M., Poupon, C. L., Changeux, J.-P., Delarue, M., and Corringer, P.-J. (2009) X-ray structure of a pentameric ligand-gated ion channel in an apparently open conformation. *Nature* **457**, 111–114
 20. Hilf, R. J. C., and Dutzler, R. (2009) Structure of a potentially open state of a proton-activated pentameric ligand-gated ion channel. *Nature* **457**, 115–118
 21. da Costa, C. J. B., Dey, L., Therien, J. P. D., and Baenziger, J. E. (2013) A distinct mechanism for activating uncoupled nicotinic acetylcholine receptors. *Nat. Chem. Biol.* **9**, 701–707
 22. Hénault, C. M., Govaerts, C., Spurny, R., Brams, M., Estrada-Mondragon, A., Lynch, J., Bertrand, D., Pardon, E., Evans, G. L., Woods, K., Elberson, B. W., Cuello, L. G., Brannigan, G., Nury, H., Steyaert, J., et al. (2019) A lipid site shapes the agonist response of a pentameric ligand-gated ion channel. *Nat. Chem. Biol.* **15**, 1156–1164
 23. Tong, A., Petroff, J. T., Hsu, F.-F., Schmidpeter, P. A., Nimigeon, C. M., Sharp, L., Brannigan, G., and Cheng, W. W. (2019) Direct binding of phosphatidylglycerol at specific sites modulates desensitization of a ligand-gated ion channel. *Elife* **8**, e50766
 24. Barrantes, F. J. (2009) Lipid matters: Nicotinic acetylcholine receptor-lipid interactions (review). *Mol. Membr. Biol.* **19**, 277–284
 25. Mouritsen, O. G., and Bloom, M. (1984) Mattress model of lipid-protein interactions in membranes. *Biophys. J.* **46**, 141–153
 26. Mouritsen, O. G., and Bloom, M. (1993) Models of lipid-protein interactions in membranes. *Annu. Rev. Biophys. Biomol. Struct.* **22**, 145–171
 27. Dumas, F., Lebrun, M. C., and Tocanne, J. F. (1999) Is the protein/lipid hydrophobic matching principle relevant to membrane organization and functions? *FEBS Lett.* **458**, 271–277
 28. Dawaliby, R., Trubbia, C., Delporte, C., Masureel, M., Antwerpen, P. V., Kobilka, B. K., and Govaerts, C. (2016) Allosteric regulation of G protein-coupled receptor activity by phospholipids. *Nat. Chem. Biol.* **12**, 35–39
 29. Wu, H., Wang, C., Gregory, K. J., Han, G. W., Cho, H. P., Xia, Y., Niswender, C. M., Katritch, V., Meiler, J., Cherezov, V., Conn, P. J., and Stevens, R. C. (2014) Structure of a class C GPCR metabotropic glutamate receptor 1 bound to an allosteric modulator. *Science* **344**, 58–64
 30. Killian, J. A., and von Heijne, G. (2000) How proteins adapt to a membrane-water interface. *Trends Biochem. Sci.* **25**, 429–434
 31. Laganowsky, A., Reading, E., Allison, T. M., Ulmschneider, M. B., Degiacomi, M. T., Baldwin, A. J., and Robinson, C. V. (2014) Membrane proteins bind lipids selectively to modulate their structure and function. *Nature* **510**, 172–175
 32. Martens, C., Stein, R. A., Masureel, M., Roth, A., Mishra, S., Dawaliby, R., Konijnenberg, A., Sobott, F., Govaerts, C., and Mchaourab, H. S. (2016) Lipids modulate the conformational dynamics of a secondary multidrug transporter. *Nat. Struct. Mol. Biol.* **23**, 744–751
 33. Norimatsu, Y., Hasegawa, K., Shimizu, N., and Toyoshima, C. (2017) Protein-phospholipid interplay revealed with crystals of a calcium pump. *Nature* **545**, 193–198
 34. Spurny, R., Ramerstorfer, J., Price, K., Brams, M., Ernst, M., Nury, H., Verheij, M., Legrand, P., Bertrand, D., Bertrand, S., Dougherty, D. A., de Esch, I. J. P., Corringer, P.-J., Sieghart, W., Lummis, S. C. R., et al. (2012) Pentameric ligand-gated ion channel ELIC is activated by GABA and modulated by benzodiazepines. *Proc. Natl. Acad. Sci. U. S. A.* **109**, E3028–E3034
 35. de Jong, D. H., Singh, G., Bennett, W. F. D., Arnarez, C., Wassenaar, T. A., Schäfer, L. V., Periole, X., Tieleman, D. P., and Marrink, S. J. (2013) Improved parameters for the Martini coarse-grained protein force field. *J. Chem. Theory Comput.* **9**, 687–697
 36. Gallivan, J. P., and Dougherty, D. A. (1999) Cation- π interactions in structural biology. *Proc. Natl. Acad. Sci. U. S. A.* **96**, 9459–9464
 37. Hénault, C. M., Juranka, P. F., and Baenziger, J. E. (2015) The M4 transmembrane α -helix contributes differently to both the maturation and function of two prokaryotic pentameric ligand-gated ion channels. *J. Biol. Chem.* **290**, 25118–25128
 38. Muller, M. P., Jiang, T., Sun, C., Lihan, M., Pant, S., Mahinthichaichan, P., Trifan, A., and Tajkhorshid, E. (2019) Characterization of lipid-protein interactions and lipid-mediated modulation of membrane protein function through molecular simulation. *Chem. Rev.* **119**, 6086–6161
 39. Duncan, A. L., Song, W., and Sansom, M. S. P. (2020) Lipid-dependent regulation of ion channels and G protein-coupled receptors: Insights from structures and simulations. *Annu. Rev. Pharmacol. Toxicol.* **60**, 31–50
 40. Arcario, M. J., Mayne, C. G., and Tajkhorshid, E. (2017) A membrane-embedded pathway delivers general anesthetics to two interacting binding sites in the *Gloeobacter violaceus* ion channel. *J. Biol. Chem.* **292**, 9480–9492
 41. Robinson, C. V., Rohacs, T., and Hansen, S. B. (2019) Tools for understanding nanoscale lipid regulation of ion channels. *Trends Biochem. Sci.* **44**, 795–806
 42. Huang, K., and El-Husseini, A. (2005) Modulation of neuronal protein trafficking and function by palmitoylation. *Curr. Opin. Neurobiol.* **15**, 527–535
 43. Keller, C. A., Yuan, X., Panzanelli, P., Martin, M. L., Alldred, M., Sassoè-Pognetto, M., and Lüscher, B. (2004) The γ 2 subunit of GABAA receptors is a substrate for palmitoylation by GODZ. *J. Neurosci.* **24**, 5881–5891
 44. Huang, C. L., Feng, S., and Hilgemann, D. W. (1998) Direct activation of inward rectifier potassium channels by PIP₂ and its stabilization by Gbetagamma. *Nature* **391**, 803–806
 45. Hansen, S. B., Tao, X., and Mackinnon, R. (2011) Structural basis of PIP₂ activation of the classical inward rectifier K⁺ channel Kir2.2. *Nature* **477**, 495–498
 46. Lacin, E., Aryal, P., Glaaser, I. W., Bodhinathan, K., Tsai, E., Marsh, N., Tucker, S. J., Sansom, M. S. P., and Slesinger, P. A. (2017) Dynamic role of the tether helix in PIP₂-dependent gating of a G protein-gated potassium channel. *J. Gen. Physiol.* **149**, 799–811

47. Long, S. B., Tao, X., Campbell, E. B., and Mackinnon, R. (2007) Atomic structure of a voltage-dependent K⁺ channel in a lipid membrane-like environment. *Nature* **450**, 376–382
48. Sands, Z. A., and Sansom, M. S. P. (2007) How does a voltage sensor interact with a lipid bilayer? Simulations of a potassium channel domain. *Structure* **15**, 235–244
49. Schmidt, D., Jiang, Q.-X., and Mackinnon, R. (2006) Phospholipids and the origin of cationic gating charges in voltage sensors. *Nature* **444**, 775–779
50. Zheng, H., Liu, W., Anderson, L. Y., and Jiang, Q.-X. (2011) Lipid-dependent gating of a voltage-gated potassium channel. *Nat. Commun.* **2**, 250
51. Laverty, D., Thomas, P., Field, M., Andersen, O. J., Gold, M. G., Biggin, P. C., Gielen, M., and Smart, T. G. (2017) Crystal structures of a GABAA-receptor chimera reveal new endogenous neurosteroid-binding sites. *Nat. Struct. Mol. Biol.* **24**, 977–985
52. Chen, Q., Wells, M. M., Arjunan, P., Tillman, T. S., Cohen, A. E., Xu, Y., and Tang, P. (2018) Structural basis of neurosteroid anesthetic action on GABAA receptors. *Nat. Commun.* **9**, 3972
53. Miller, P. S., Scott, S., Masiulis, S., Colibus, L. D., Pardon, E., Steyaert, J., and Aricescu, A. R. (2017) Structural basis for GABAA receptor potentiation by neurosteroids. *Nat. Struct. Mol. Biol.* **24**, 986–992
54. Nury, H., Renterghem, C. V., Weng, Y., Tran, A., Baaden, M., Dufresne, V., Changeux, J.-P., Sonner, J. M., Delarue, M., and Corringer, P.-J. (2011) X-ray structures of general anaesthetics bound to a pentameric ligand-gated ion channel. *Nature* **469**, 428–431
55. Price, K. L., and Lummis, S. C. R. (2005) FlexStation examination of 5-HT₃ receptor function using Ca²⁺ - and membrane potential-sensitive dyes: Advantages and potential problems. *J. Neurosci. Methods* **149**, 172–177
56. Nowak, M. W., Gallivan, J. P., Silverman, S. K., Labarca, C. G., Dougherty, D. A., and Lester, H. A. (1998) *In vivo* incorporation of unnatural amino acids into ion channels in *Xenopus* oocyte expression system. *Methods Enzymol.* **293**, 504–529
57. Rupakheti, C. R., Roux, B., Dehez, F., and Chipot, C. (2018) Modeling induction phenomena in amino acid cation- π interactions. *Theor. Chem. Acc.* **137**, 174
58. Khan, H. M., Souza, P. C. T., Thallmair, S., Barnoud, J., de Vries, A. H., Marrink, S. J., and Reuter, N. (2020) Capturing choline-aromatics cation- π interactions in the MARTINI force field. *J. Chem. Theory Comput.* **16**, 2550–2560
59. Qi, Y., Ingólfsson, H. I., Cheng, X., Lee, J., Marrink, S. J., and Im, W. (2015) CHARMM-GUI Martini maker for coarse-grained simulations with the Martini force field. *J. Chem. Theory Comput.* **11**, 4486–4494
60. Jo, S., Kim, T., Iyer, V. G., and Im, W. (2008) CHARMM-GUI: A Web-Based Graphical User Interface for CHARMM, John Wiley & Sons, Inc, Hoboken, NJ
61. Yesylevskyy, S. O., Schäfer, L. V., Sengupta, D., and Marrink, S. J. (2010) Polarizable water model for the coarse-grained MARTINI force field. *PLoS Comput. Biol.* **6**, e1000810
62. Abraham, M. J., Murtola, T., Schulz, R., Páll, S., Smith, J. C., Hess, B., and Lindahl, E. (2015) Gromacs: High performance molecular simulations through multi-level parallelism from laptops to supercomputers. *SoftwareX* **1–2**, 19–25
63. McGibbon, R. T., Beauchamp, K. A., Harrigan, M. P., Klein, C., Swails, J. M., Hernández, C. X., Schwantes, C. R., Wang, L.-P., Lane, T. J., and Pande, V. S. (2015) MDTraj: A modern open library for the analysis of molecular dynamics trajectories. *Biophys. J.* **109**, 1528–1532
64. Michaud-Agrawal, N., Denning, E. J., Woolf, T. B., and Beckstein, O. (2011) MDAAnalysis: A toolkit for the analysis of molecular dynamics simulations. *J. Comput. Chem.* **32**, 2319–2327
65. Wassenaar, T. A., Pluhackova, K., Böckmann, R. A., Marrink, S. J., and Tieleman, D. P. (2014) Going backward: A flexible geometric approach to reverse transformation from coarse grained to atomistic models. *J. Chem. Theory Comput.* **10**, 676–690
66. Huang, J., Rauscher, S., Nawrocki, G., Ran, T., Feig, M., de Groot, B. L., Grubmüller, H., and MacKerell, A. D. (2017) CHARMM36m: An improved force field for folded and intrinsically disordered proteins. *Nat. Methods* **14**, 71–73
67. Khan, H. M., MacKerell, A. D., and Reuter, N. (2019) Cation- π interactions between methylated ammonium groups and tryptophan in the CHARMM36 additive force field. *J. Chem. Theory Comput.* **15**, 7–12
68. Essman, U., Perera, L., Berkowitz, M. L., Darden, T., Lee, H., and Pedersen, L. G. (1995) A smooth particle mesh ewald potential. *J. Chem. Phys.* **103**, 8577–8593
69. Hess, B. (2008) P-LINCS: A parallel linear constraint solver for molecular simulation. *J. Chem. Theory Comput.* **4**, 116–122
70. Parrinello, M., and Rahman, A. (1981) Polymorphic transitions in single crystals: A new molecular dynamics method. *J. Appl. Phys.* **52**, 7182–7190
71. Bussi, G., Donadio, D., and Parrinello, M. (2007) Canonical sampling through velocity rescaling. *J. Chem. Phys.* **126**, 014101
72. Knoflach, F., Hernandez, M.-C., and Bertrand, D. (2018) Methods for the discovery of novel compounds modulating a gamma-aminobutyric acid receptor type A neurotransmission. *J. Vis. Exp.* <https://doi.org/10.3791/57842>